ACS Photonics

pubs.acs.org/journal/apchd5

Article

Third-Order Nonlinear Optical Properties and Saturation of Two-Photon Absorption in Lead-Free Double Perovskite Nanocrystals under Femtosecond Excitation

Aamir Mushtaq,[#] Bapi Pradhan,[#] Dushyant Kushavah, Yiyue Zhang, Mathias Wolf, Nadine Schrenker, Eduard Fron, Sara Bals, Johan Hofkens, Elke Debroye, and Suman Kalyan Pal*

Cite This: https://doi.org/10.1021/acsphotonics.1c01351

ABSTRACT: Lead halide perovskites have been widely explored in the field of photovoltaics, light-emitting diodes, and lasers due to their outstanding linear and nonlinear optical (NLO) properties. But, the presence of lead toxicity and low chemical stability remain serious concerns. Lead-free double perovskite with excellent optical properties and chemical stability could be an alternative. However, proper examination of the NLO properties of such a material is crucial to identify their utility for future nonlinear device applications. Herein, we have made use of femtosecond (fs) Z-scan technique to explore the NLO properties of $Cs_2AgIn_{0.9}Bi_{0.1}Cl_6$ nanocrystals (NCs). Our measurements suggest that under nonresonant fs excitation, perovskite NCs exhibit strong two-photon absorption (TPA). The observed saturation of TPA at high light intensities has been explained by a customized model. Furthermore, we have demonstrated a change in the nonlinear refractive index of the NCs under varying input intensities. The strong TPA absorption of lead-free double perovskite NCs could be used for Kerr nonlinearity-based nonlinear applications such as optical shutters for picosecond lasers.

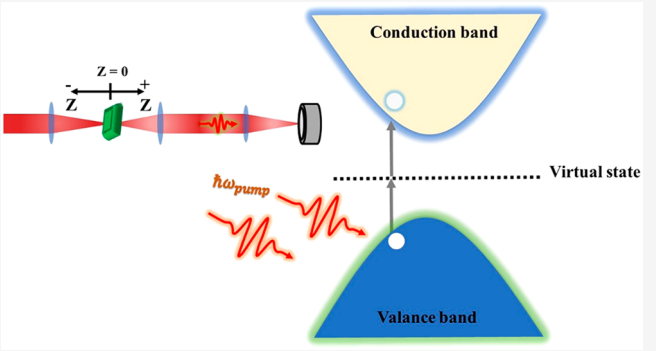

KEYWORDS: *Z-scan, TPA saturation, double perovskite, nonlinear optics, nonlinear refractive index*

Strong interaction of intense light with matter comes under the class of nonlinear optics, which becomes extremely important for modern technologies. The nonlinear optical properties of a specific material play an important role in revealing light−matter interactions and ultrafast dynamics.[1,2] Formation of new secondary optical fields and variation of phase and frequency instigated by polarization made the NLO effect a keystone for the manipulation of photons in advanced technologies such as optical computation, information processing and storage, and telecommunication.[3−6] The NLO effect has been identified in a series of materials including transition metal dichalcogenides (TMDCs),[7,8] graphene,[9,10] hexagonal boron nitride (h-BN),[11] and metal organic frameworks (MOFs).[12,13] The materials possessing optical nonlinearities find applications in optical switches, optical data storage,[14,15] and lasers.[16] Nowadays, switching of optical signals in optical communication is achieved through optical-to-electronic-to-optical (OEO) transmutation components. Operation of such photonic devices is based on the instantaneous Kerr effect, which occurs when bound electronic charges of material are virtually excited by photons having energies less than the bandgap resulting in change in refractive index of the material.[17] The Kerr effect in thin films is generally weak, and in that case direct single or multiphoton absorption process can bring the change in refractive index that is significantly larger than the change due to Kerr effect. In contrast, the linear electro-optic or Pockels effect (a second order process) where the change in refractive index varies linearly with the electric field (of laser beam) finds application in electro-optic modulators. However, due to intrinsic centrosymmetric structures, traditional perovskites ($CsPbX_3$ or $MAPbX_3$) are not useful for applications based on the Pockels effect.[18] A recent report shows that germanium based perovskite ($CsGeI_3$) exhibits an electro-optic coefficient which is better than that of $LiNbO_3$.[19] It is worth mentioning that the optical Kerr effect is present in all centrosymmetric media, but the strength of this effect is weaker than the linear electro-optic effect. Furthermore, carrier induced third-order nonlinearities depend on carrier diffusion length and recombination of carriers in a material.

Received: September 4, 2021

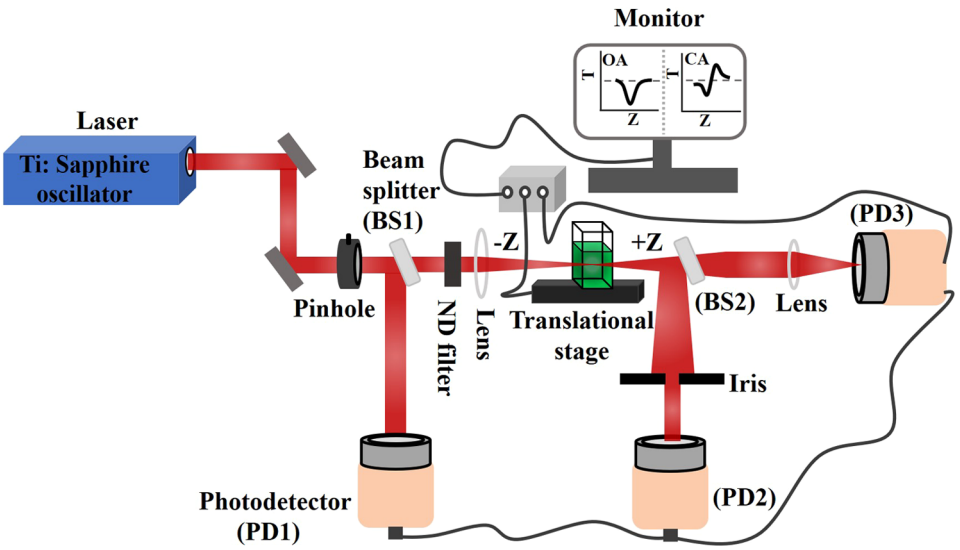

Figure 1. Cartoon depicting schematic of Z-scan setup.

Metal halide perovskites (MHPs) exhibit remarkable optoelectronic properties like high absorption coefficients, long carrier diffusion lengths, and high photoluminescence (PL) intensities.[20,21] Moderate exciton binding energies[22] and tunable bandgaps along with rich structural and chemical diversity of halide perovskites enable their application in varieties of photonic[23] and optoelectronic devices like lasers,[24,25] photodetectors, and LEDs.[26,27] According to recent reports, all inorganic $CsPbBr_3$ perovskite NCs possess a remarkable TPA cross-section ($\sim 10^5$ GM).[28,29] Moreover, the rich structural diversity of 2D hybrid organic−inorganic perovskites makes them useful for optics and optoelectronics applications.[30] Apart from these, hybrid organic−inorganic metal halide perovskite ($CH_3NH_3PbX_3$, X = Br, Cl, I) NC films exhibit strong nonlinear optical properties in the mid-IR region.[31] Ni-doped $CsPbI_3$ NCs have been shown to possess a strong TPA cross-section (10^4 GM) with a TPA coefficient and nonlinear refractive index of the order of 10^{-11} cm/W and 10^{-12} cm^2/W, respectively.[32] Despite these superior properties, lead toxicity and low chemical stability of these perovskites remain a concern, which requires the exploration of new lead-free perovskites to alleviate these issues.

Several methods have been adopted to replace lead from MHPs. Initially, tin (Sn) was used as substitute; however, Sn-based perovskites are extremely unstable under ambient conditions due to facile oxidation of Sn^{2+} to Sn^{4+}.[33−35] Further, lead-free perovskites based on Bi^{3+} and Sb^{3+} possess an indirect bandgap.[36,37] Double perovskites with a general formula of $A_2BB^*X_6$ (where B and B* are two size compatible cations, A is a monovalent cation and X is a halide), on the other hand, could prove to be a more stable alternative of conventional MHPs. The nonlinear optical properties of this class of perovskites still need to be explored in order to utilize them in nonlinear optical devices. In the present work, we explore third-order nonlinear optical properties of $Cs_2AgIn_{0.9}Bi_{0.1}Cl_6$ double perovskite NCs in the fs regime by exploiting open aperture (OA) and closed aperture (CA) Z-scan techniques.

EXPERIMENTAL METHODS

The Z-scan setup (Figure 1) used in this work has been previously described elsewhere.[38] In brief, a Ti:sapphire regenerative amplifier (Spitfire ace, Spectra Physics) seeded by an oscillator (Mai Tai SP, Spectra Physics) was used as a light source. A fraction of the laser output from the amplifier having a central wavelength 800 nm and a pulse width 57 fs was used for measurement. To record intensities of reference and sample signals, we split the beam into two parts with the help of a beam splitter (BS1). Then one beam finds its path to photodetector PD1 (reference detector) and second one passes through the sample and again gets divided into two beams at beam splitter BS2. Finally, one beam goes into photodetector PD2 (close aperture configuration) and the second beam into photodetector PD3 (open aperture configuration). The laser beam was focused over the sample using a convex lens with a focal length of 10 cm. The beam waist was measured using a sensor and found to be 37−40 μm at the focus. A computer controlled translational stage was used for scanning the samples. In each scan, sample was moved to the positive and negative sides of $Z = 0$ position. The optical powers were measured using a power meter (Model No. 1917-R) from Newport, USA. Z-scan curves were fitted using the MATLAB and OriginLab programs.

RESULTS AND DISCUSSION

Double perovskite $Cs_2AgIn_{0.9}Bi_{0.1}Cl_6$ NCs were synthesized according to a room-temperature antisolvent precipitation method (see Supporting Information) and characterized structurally and optically. Figure 2(a,b) shows low and high resolution TEM images of NCs along with their size distribution (inset of Figure 2(a)). The average particle size was found to be 3.5 nm. The crystal lattice of NCs can be clearly viewed from the high-resolution scanning transmission electron microscopy (HRSTEM) image (Figure 2(b,c)). The fast Fourier transform (FFT) in Figure 2(d) reveals a fcc structure of double perovskite NCs and shows that the NC depicted in Figure 2(b) is oriented in the [111] zone axis (ZA). The crystal structure of the double perovskites agrees well with the known structure for $Cs_2AgInCl_6$ in literature.[39] XRD and XPS measurements (Figure S1(a,b), Supporting

https://doi.org/10.1021/acsphotonics.1c01351
ACS Photonics XXXX, XXX, XXX−XXX

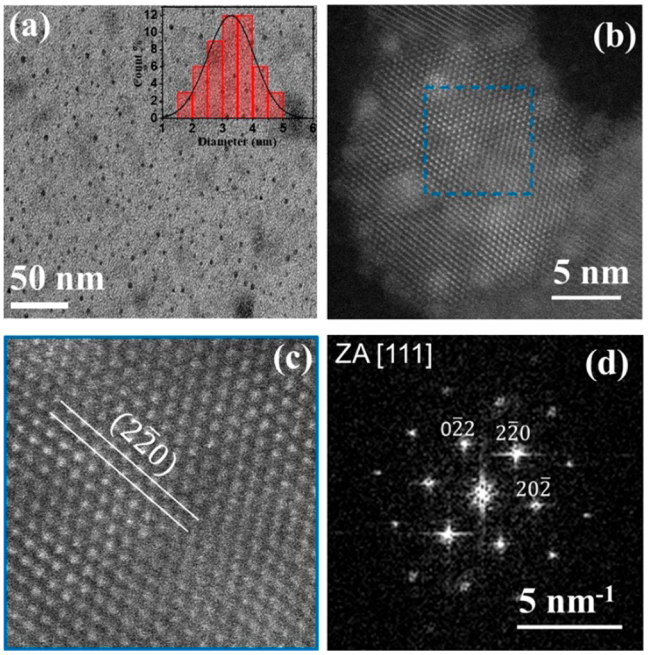

Figure 2. (a) TEM images of double perovskite NCs (inset represents histogram of particle size distribution). (b) HRSTEM image of a double perovskite NC. (c) Close-up of the area marked with a blue square in panel (b). The direction of the (2−20) planes are indicated by white lines. (d) FFT of the NC in panel (b) showing the [111] ZA.

Information) further confirm the formation of NCs as described in previous reports.[40] The EDX elemental maps (Figure S1(c), Table S1, Supporting Information) for Cs, Ag, In, Bi, and Cl, which were taken from the double perovskite NCs, additionally confirm the composition of the NCs.

Figure 3(a) depicts the absorption spectrum of NCs in solution having a peak around 370 nm. The bandgap of the NCs was estimated from the Tauc plot (Inset of Figure 3(a)) and found to be 3.0 eV. We recorded the corrected (see Supporting Information for details on the correction method) photoluminescence (PL) spectrum of the NC film exhibiting a broad orange colored emission with a maximum at 630 nm as shown in Figure 3(b). Note that the uncorrected PL spectrum of the NCs (Figure S3(a), Supporting Information) is very similar to the existing report.[40] The origin of such emission has been reported to be the relaxation of charge carriers from allowed direct band states to forbidden states.[40] Further, a transient PL measurement was performed using time-correlated single-photon counting (TCSPC) by exciting the sample with 355 nm laser pulses in the microsecond time window (Figure 3(c)). We fitted the curve using a biexponential function and found two time components; 40 ns (98.4%) and 308 ns (1.6%). The long lifetime component could be ascribed to parity forbidden transitions from the conduction band minimum to the valence band maximum.[41]

Next, we drop casted presynthesized NCs on a glass coverslip followed by drying. The average thickness of the NC film was measured to be 512 nm using scanning electron microscopy (SEM) (Figure S2, Supporting Information).

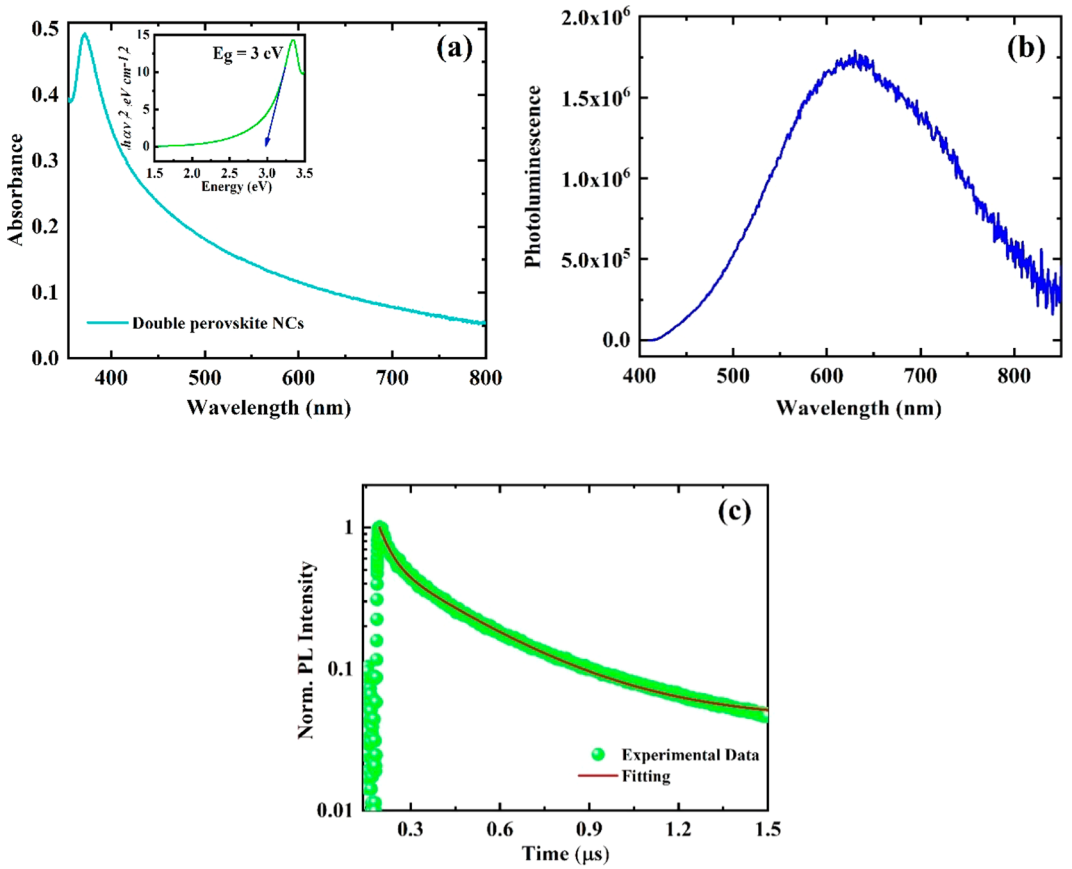

Figure 3. Absorption (a) and corrected photoluminescence (b) spectra of the double perovskite NCs. (c) PL decay trace of NCs recorded using TCSPC. Inset of (a) represents the Tauc plot.

https://doi.org/10.1021/acsphotonics.1c01351
ACS Photonics XXXX, XXX, XXX−XXX

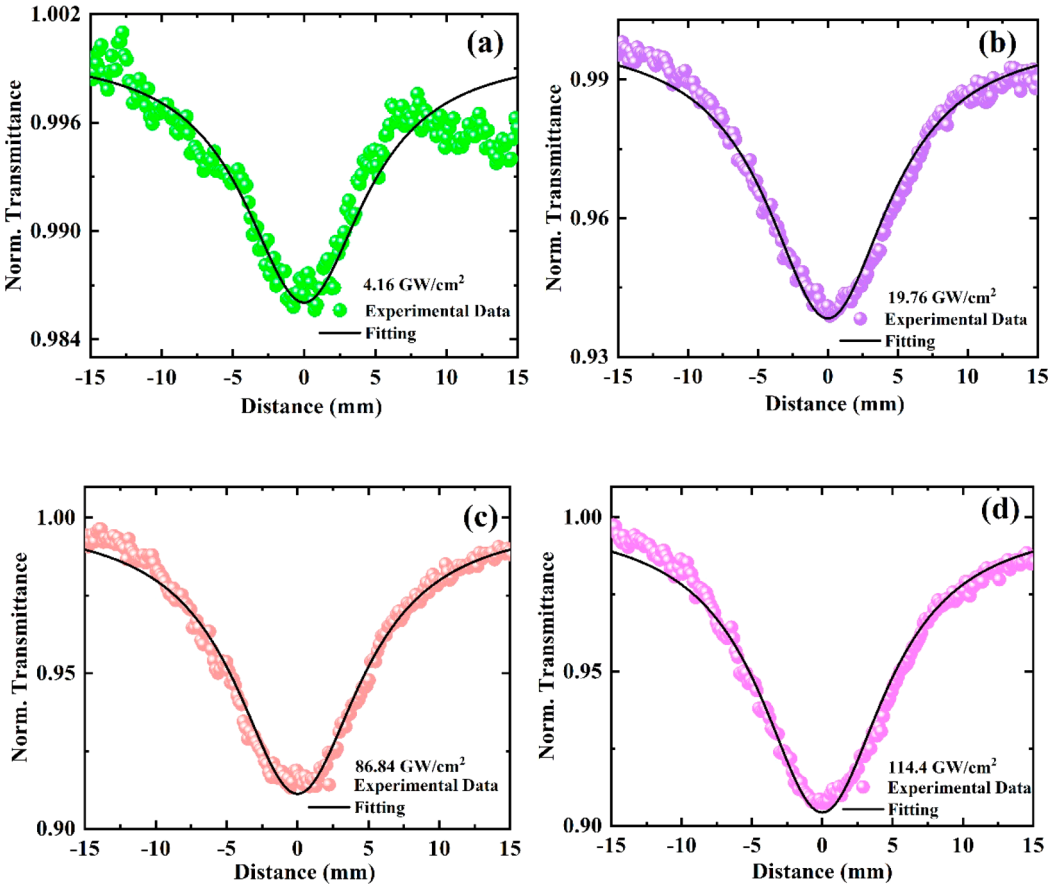

Figure 4. Open aperture (OA) Z-scan curves obtained at different input intensities: (a) 4.16, (b) 19.76, (c) 86.84, and (d) 114.4 GW/cm^2 at 800 nm following fs excitation.

Table 1. NLO Coefficients (TPA Cross-Section along with Real and Imaginary Parts of Susceptibility and Optical Limiting Onsets) of NCs

S. No.	I_0 (GW/cm^2)	$\beta \times 10^{-9}$ (cm/W)	$n_2 \times 10^{-13}$ (cm^2/W)	$\sigma_{TPA} \times 10^4$ (GM)	Re$\chi^{(3)} \times 10^{-11}$ (m^2/W)	IM$\chi^{(3)} \times 10^{-11}$ (m/W)	limiting offset (mJ/cm^2)
1	4.16	66.43	–	3.11	–	14	0.06
2	19.76	64.93	–	3.0	–	13.6	0.15
3	86.84	21.90	2.6	1.02	1.37	4.60	0.7
4	114.4	18.061	2.4	0.84	1.26	3.79	1.5
5	301.6	6.88	0.55	0.32	0.29	1.44	2.6
6	497.12	4.322	−0.79	0.20	−4.15	0.90	5.9

Symmetric transmission curves shown in Figure 4 and S4 (Supporting Information) are OA Z-scan traces for NCs measured at 800 nm. As the input intensity increases, the transmission through the sample decreases and finally saturates at higher input intensities (Figure 4). Clearly, the data obtained at different input intensities indicate a reverse saturable absorption (RSA) behavior of perovskite NCs. We kept the incident light intensities during the experiments to an optimal level to avoid supercontinuum generation and repeated the scan multiple times. Since the energy of the excitation light (1.55 eV) is below the bandgap (3.0 eV) of the NCs, the direct transition of electrons to the conduction band via one-photon absorption is not feasible. In fact, the absorption spectrum of the perovskite NCs film (Figure S3(b), Supporting Information) shows that the one-photon absorption at 800 nm is negligible. The only means left for electrons to reach the conduction band is via two-photon absorption. Therefore, the observed optical nonlinearity at nonresonant excitation (at 800 nm) could be ascribed to the generation of bound or free carriers via two-photon absorption processes.

To extract the TPA absorption coefficient, we have made use of the multiphoton absorption model,[42]

$$T_{OA(nPA)} = \frac{1}{\left[1 + (n-1)\alpha_n L_{eff}\left(\frac{I_0}{1+\left(\frac{z}{z_0}\right)^2}\right)^{n-1}\right]^{1/n-1}} \quad (1)$$

where $L_{eff} = \frac{1-e^{-\alpha_0 L}}{\alpha_0}$ is the effective path length of the sample, α_0 is the linear absorption coefficient of the sample, $z_0 = \frac{\pi w_0^2}{\lambda}$ is the Rayleigh range, which is calculated to be 4.8 mm, w_0 is the beam width at the focus and calculated to be 33.05 μm, and I_0 is the input peak intensity at the focus. The calculated value of

https://doi.org/10.1021/acsphotonics.1c01351
ACS Photonics XXXX, XXX, XXX−XXX

effective path length (512 nm) is found to be much less than Rayleigh range (z_0), satisfying the thin film approximation $L_{eff} \ll z_0$.

OA data are fitted well using eq 1 with $n = 2$. The calculated values of the TPA coefficient (i.e., α_2 which is also assigned to β) are of the order of 10^{-9} cm/GW and are given in Table 1. It is noteworthy to mention that no nonlinearity has been observed from the glass coverslip at the highest input intensities used (Figure S4(c), Supporting Information).

Further, to validate the TPA response of our sample, we measured fluorescence following 800 nm laser excitation (Figure 5). The NC film exhibits a broad emission band

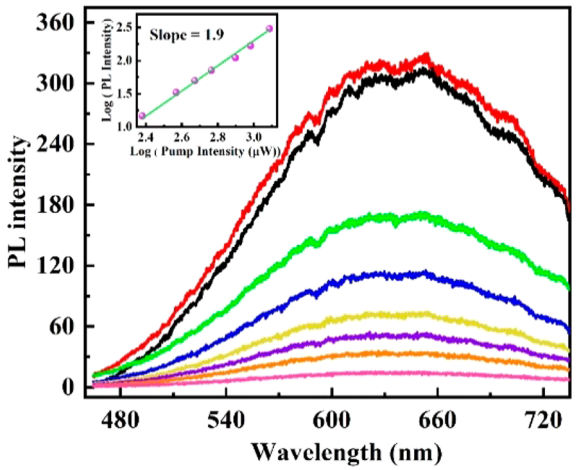

Figure 5. Fluorescence spectra of NCs film at different excitation intensities at 800 nm: 1510 μW (red curve), 1220 μW (black curve), 960 μW (green curve), 790 μW (blue curve), 580 μW (yellow curve), 470 μW (purple curve), 370 μW (orange curve), and 240 μW (pink curve). The inset represents the logarithmic plot of excitation-power dependent PL.

with a maximum around 630 nm. It is worth mentioning that the observed two-photon PL is consistent with the one observed following high energy (3.2 eV) single-photon excitation as shown in Figure 3(b). Since the linear absorption at 800 nm is negligible, the observed fluorescence is attributed to TPA. To further confirm the TPA process, the power dependent fluorescence intensity of our sample was measured. The logarithmic plot of the fluorescence intensity versus input power with a slope of 1.9 (inset of Figure 5) further indicates that the mechanism responsible for the observed emission at 800 nm excitation is TPA.

We calculated the TPA cross-section (σ_{TPA}) using the following equation[42]

$$\sigma_{TPA} = \frac{(h\omega)}{N}\beta \tag{2}$$

Here, ω is the frequency of laser radiation and N is the concentration of NCs. Obtained values of the TPA cross-section are in the range of 10^4 GM (Table 1).

To account for the optical limiting effect, transmission curves are drawn as a function of the input fluence at each excitation intensity (Figure S5, Supporting Information). The light fluence $F(z)$ at any position z of the incident beam with energy E_{in} was calculated from the expression[43]

$$F(z) = \frac{4\sqrt{\log 2}\,E_{in}}{\pi^{3/2}w(z)^2} \tag{3}$$

where the beam radius $w(z)$ is given by

$$w(z) = w(0)[1 + (z/z_0)^2]^{1/2} \tag{4}$$

The decrease in the transmission with the increase in input fluence (Figure S5, Supporting Information) demonstrates the optical limiting behavior of perovskite NCs. The optical limit offset at which transmission starts to decrease substantially represents the optical limiting quality of a material. The values of the optical limiting offset of the double perovskite NCs are presented in Table 1.

Next, Figure 6 represents the closed-aperture (CA) measurements performed on the NCs. The CA curves exhibit a valley−peak type structure. The observed prefocal transmission minimum (valley) followed by a transmission maximum (peak) bears the Z-scan signature of positive refractive nonlinearity (with the nonlinear refractive index, $n_2 > 0$).

To extract the values of n_2, CA traces were fitted using the following analytically derived equation[44]

$$T_{CA} = 1 + \frac{4x\Delta\phi_0}{(x^2+9)(x^2+1)} - \frac{2(x^2+3)\Delta\psi_0}{(x^2+9)(x^2+1)} \tag{5}$$

Here, $\Delta\phi_0 = kn_2I_0L_{eff}$ is the on-axis phase shift at the focus, $k = \frac{2\pi}{\lambda}$, $\Delta\psi_0 = \frac{\beta I_0 L_{eff}}{2}$ is the phase change due to nonlinear absorption, β is the two-photon absorption coefficient, and $x = \frac{z}{z_0}$. Good fitting of the CA curves with eq 5 infers that the asymmetric transmission behavior in NCs could be due to strong TPA.[45] The estimated value of n_2 is in the range of $0.55-2.6 \times 10^{-13}$ cm^2/W (Table 1). We must note that the fitting of the CA data is not as good as the OA Z-scan. The fitting error could be attributed to the presence of a second peak in the CA Z-scan curve at ∼9 mm (Figure 6(a,b)). Actually, the nonuniformity in the film thickness causes the distortion of Gaussian profile of the laser beam and thereby induces such artifact in the CA profile.[46] Overall errors in these measurements and hence in the values of NLO coefficients are estimated to be ±10−15% and may arise mainly from input laser fluctuation, estimating peak intensities and fitting errors.

The real and imaginary parts of the third-order nonlinear susceptibility were calculated using the following relations[47]

$$\mathrm{Re}\chi^{(3)}(esu) = \frac{cn_0^2}{120\pi^2}n_2\left(\frac{\mathrm{m}^2}{\mathrm{W}}\right) \tag{6}$$

$$\mathrm{Im}\,\chi^{(3)}(esu) = \frac{c^2n_0^2}{240\pi^2\omega}\beta\left(\frac{\mathrm{m}}{\mathrm{W}}\right) \tag{7}$$

Here, n_0 is the linear refractive index and c is the speed of the light. Since the exact value of n_0 for $Cs_2AgIn_{0.9}Bi_{0.1}Cl_6$ NCs is unknown, we have used the value $n_0 = 1.44$ of the same class of material as reference.[48] The calculated values of n_2 are listed in Table 1.

To extract the superior nonlinear optical behavior of the double perovskite NCs, a comparison of the NLO parameters is made with the reported materials (Table 2). Clearly, the TPA coefficient of $Cs_2AgIn_{0.9}Bi_{0.1}Cl_6$ NCs is ∼2−3 orders of magnitude larger than InP/ZnS quantum dots (QDs) and 5 orders of magnitude larger than ZnSe QDs. The TPA cross-

https://doi.org/10.1021/acsphotonics.1c01351
ACS Photonics XXXX, XXX, XXX−XXX

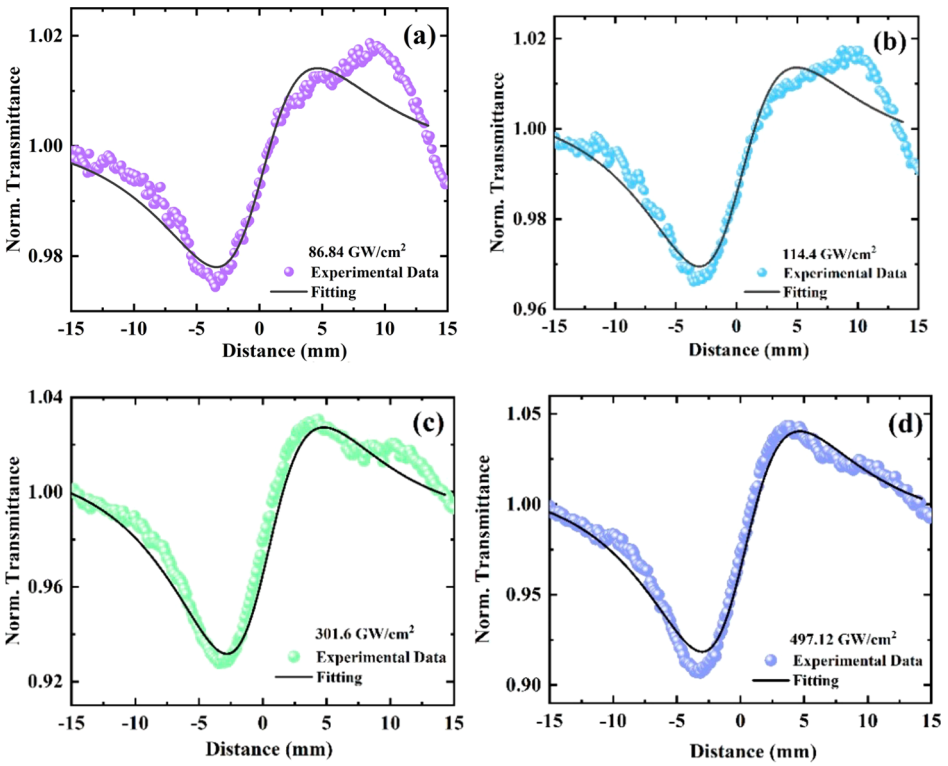

Figure 6. Closed-aperture (CA) Z-scan curves obtained with fs laser excitation at 800 nm having different intensities.

Table 2. Comparison of NLO Properties of Double Perovskite NCs with Other Nanomaterials

material	excitation	β (cm/W)	n_2 (cm^2/W)	σ_{TPA} (GM)	ref
$Cs_2AgIn_{0.9}Bi_{0.1}Cl_6$	800 nm, 1 kHz, 58 fs	21.90×10^{-9}	2.6×10^{-13}	1.02×10^4	present work
$CsPbBr_3$ NCs	800 nm, 1 kHz, 70 fs	180×10^{-11}	10^{-9}	98×10^4	54
$CsPbBr_3$ nanorods	800 nm, 1 kHz, 70 fs	0.71×10^{-11}	–	0.2×10^4	54
$CsPbBr_3$ 0.03% and 0.05% Ni doped	800 nm, 1 kHz, 70 fs	3.8×10^{-11}	7.9×10^{-12}	1.56×10^4	32
		3.9×10^{-11}	8.4×10^{-11}	1.6×10^4	
$CsPbCl_2Br$	800 nm, 1 kHz, 50 fs	5.4×10^{-11}	–	1.1×10^5	55
$CsPbClBr_2$		6.4×10^{-11}	–	1.6×10^5	
$CsPbBr_3$ QDs		9.1×10^{-11}	–	2.2×10^5	
Fe^{3+} doped $CsPb(Cl/Br)_3$ microwires	800 nm, 1 kHz, 140 fs	210×10^{-9}	–	–	56
$CsPbBr_3$ R-Perov-NC	800 nm, 1 kHz, 100 fs	–	–	3.68×10^4	57
$CH_3NH_4PbBr_3$ Single crystal	800 nm, 1 kHz, 140 fs	8.6×10^{-9}	–	–	58
CdSeTe QDs	800 nm, 1 kHz, 120 fs				59
4 nm		4.2×10^{-10}	–	–	
5 nm in size		3.55×10^{-9}	–	–	
ZnSe QDs 4.5 nm in size	800 nm, 10 Hz, 100 fs	7.9×10^{-14}	–	0.49×10^4	60
ZnSe/ZnS	800 nm, 10 Hz, 100 fs	8.2×10^{-14}		0.51×10^4	60
Core/shell 4.5 nm in size				–	
CuS QDs	800 nm, 10 kHz, 100 fs	2.3×10^{-12}	–	–	61
InP/ZnS QDs	800 nm, 1 kHz, 100 fs				51
2.2 nm		9.0×10^{-12}	-0.57×10^{-15}	3.5×10^3	
2.8 nm in size		1.2×10^{-11}	-0.71×10^{-15}	6.2×10^3	

section is found to be a few orders of magnitude higher than InP/ZnS QDs and CdTe QDs.[49] Similarly, the TPA coefficient of our perovskite NCs is much larger than $CsPbBr_3$ NCs and nanorods, and $CsPb(Cl_{0.53}Br_{0.47})_3$ NCs.[50] It is apparent from Table 2 that the value of the TPA coefficient of our NCs is higher than alternative materials. The lower value of the TPA cross-section of the double perovskite NCs could be the consequence of a reduced density of states due to large quantum confinement in small sized particles.[51]

Figure 7(a) depicts the variation of the TPA coefficient as a function of the input intensity. It is inferred from the figure that with an increase in input fluence, β decreases and tends to saturate at higher intensities. Nonetheless, n_2 decreases with the increment of intensity (Table 1) due to its direct dependence on the charge carrier density. In fact, the effective nonlinear refractive index is given by the following relation[52]

$$n_2^* = n_2 + \frac{\xi_\gamma N(t)}{I} \tag{8}$$

https://doi.org/10.1021/acsphotonics.1c01351
ACS Photonics XXXX, XXX, XXX−XXX

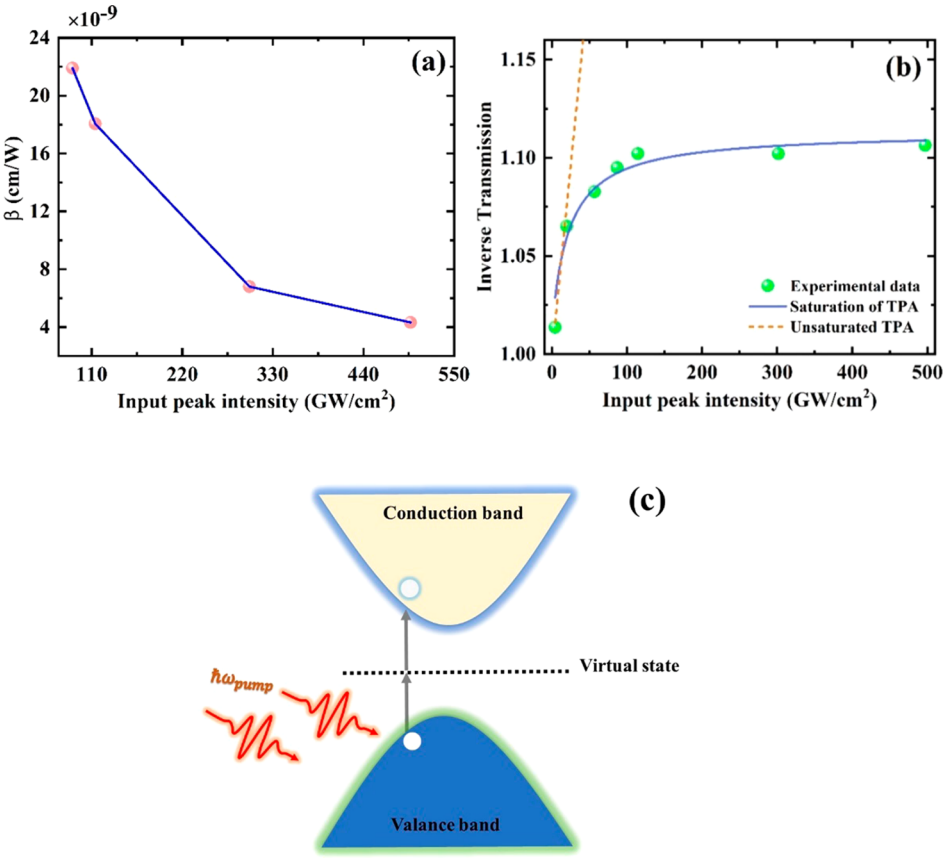

Figure 7. (a) Variation of TPA coefficient (β) as a function of the peak intensity of the input light. (b) Plot of inverse transmission vs input peak intensity fitted with saturation (solid blue line) and nonsaturation TPA (dotted orange line) models. (c) Schematic of the TPA process in double perovskite NCs under light (800 nm) illumination.

Here, n_2^* is the effective nonlinear refractive index, $N(t)$ is the photoexcited carrier density, ξ_γ is the change in refractive index per unit density of conduction band electrons, and I is the input intensity. Free carriers can alter the refractive index because of their capability to absorb light.[53] In nonresonant excitation, the dominant pathway for the generation of free carriers is multiphoton absorption, whereas in resonant conditions, the generation takes place via linear absorption.

In case of nonresonant (fs) excitation, the low intensity regime contribution to the nonlinearity is assigned to bound charge carriers, while at a high intensity regime, the nonlinearity from free carriers dominates because free charge carriers accumulate during the pulse.[62] On the contrary, for nanosecond pulses, free carriers disguise the contribution from bound electronic charges and become primary contributors to optical nonlinearity. In the low intensity regime, the TPA is weak and $N(t)$ is almost constant; therefore, an increase in excitation power causes n_2^* to decrease in accordance with eq 8. However, in the high intensity regime, the growth of $N(t)$ is slowly counterbalanced with the increase of the excitation intensity and n_2^* decreases again with the increase of excitation intensity. It is worth noting that we have taken into account the contribution of the nonlinear refraction from the coverslip by subtracting its value from the sample. At the highest intensity (497.12 GW/cm^2), the negative value of n_2 is due to decreased transmission ($\Delta T_{P-V} = T_{peak} - T_{valley}$) of NCs as compared to the coverslip (Figure S6, Supporting Information).[50,51]

To examine the observed saturation of TPA in more detail, we utilized an alternative technique. We measured the transmitted intensity at each incident peak intensity by directly placing the sample at the beam waist of a focused laser beam. Figure 7(b) represents the plot of the inverse transmission vs intensity for the NCs. A typical TPA feature, i.e., inverse transmission, increases as the input intensity gradually increases, is observed. Light attenuation for degenerate TPA in a material is described by[58]

$$\frac{dI(z)}{dz} = -\alpha_0 I(z) - \beta I^2(z) \tag{9}$$

where $I(Z)$ is the peak intensity, α_0 is the linear absorption coefficient, and β is the TPA coefficient. The solution of the above differential equation can be expressed as[58]

$$T(I) = \frac{e^{-\alpha_0 L}}{\beta I L_{eff} + 1} \tag{10}$$

Here, L is the path length and L_{eff} is the effective path length. The equation above can more accurately be expressed by taking into account possible reflection and scattering, which lead to the reduction of light intensity entering the sample by the factor $(1 - R)$, where R is the reduction factor caused by scattering and reflection, as[63]

$$T(I) = \frac{(1-R)^2 e^{-\alpha_0 L}}{(1-R)\beta I L_{eff} + 1} \tag{11}$$

https://doi.org/10.1021/acsphotonics.1c01351
ACS Photonics XXXX, XXX, XXX−XXX

In the low-intensity regime, inverse transmission increases linearly (Figure 7(b)) in accordance with eq 11 conforming the presence of TPA. On increasing the intensity further, the transmission through the sample becomes stabilized giving a signature of TPA saturation. In this scenario, the TPA coefficient can be expressed as[64]

$$\beta(I) = \frac{\beta_0}{1 + \frac{I}{I_{sat}}} \tag{12}$$

Here, β_0 is the nonsaturation TPA coefficient and I_{sat} is the saturation intensity. The nonsaturation TPA model (eq 11) alone was unable to fit the experimental data (dotted line in Figure 7(b)). Therefore, we combined both the TPA saturation model (eq 12) and eq 11 to support our data. Eqs 11 and 12 together fit the experimental data well as shown in Figure 7(b). The value of β_0 obtained from fitting is 74.32 cm/GW and the corresponding TPA saturation intensity is 23.11 GW/cm^2. The mechanism of the TPA process is schematically shown in Figure 7(c).

CONCLUSIONS

In this work, we have investigated third-order nonlinear optical properties of $Cs_2AgIn_{0.9}Bi_{0.1}Cl_6$ double perovskite NCs in the femtosecond regime by employing a Z-scan technique. Under nonresonant excitation, observed nonlinearities are attributed to bound charges generated in the low-intensity regime. However, at higher intensities, nonlinearity is due to free carriers and the TPA process. The nonlinear refractive index of perovskite NCs decreases with the increase of excitation intensity due to the variation in charge carrier density. Furthermore, we observe the saturation of TPA in the perovskite NCs. The large values of the TPA coefficient and cross-section demonstrate the prospect of this material for applications involving multiphoton bioimaging and upconverted lasing.

ASSOCIATED CONTENT

Supporting Information

The Supporting Information is available free of charge at https://pubs.acs.org/doi/10.1021/acsphotonics.1c01351.

Synthesis of NCs, experimental details, SEM image of NC film, optical limiting curves of perovskite NCs, OA and CA Z-scan data of coverslip (PDF)

AUTHOR INFORMATION

Corresponding Author

Suman Kalyan Pal − *School of Basic Sciences and Advanced Material Research Center, Indian Institute of Technology Mandi, Kamand 175005 HP, India;* orcid.org/0000-0003-2498-6217; Email: suman@iitmandi.ac.in

Authors

Aamir Mushtaq − *School of Basic Sciences and Advanced Material Research Center, Indian Institute of Technology Mandi, Kamand 175005 HP, India;* orcid.org/0000-0003-1845-8266

Bapi Pradhan − *Department of Chemistry, KU Leuven, 3001 Heverlee, Belgium;* orcid.org/0000-0002-6202-7343

Dushyant Kushavah − *School of Basic Sciences and Advanced Material Research Center, Indian Institute of Technology Mandi, Kamand 175005 HP, India;* orcid.org/0000-0001-5745-9435

Yiyue Zhang − *Department of Chemistry, KU Leuven, 3001 Heverlee, Belgium*

Mathias Wolf − *Department of Chemistry, KU Leuven, 3001 Heverlee, Belgium;* orcid.org/0000-0002-5228-9454

Nadine Schrenker − *Electron Microscopy for Materials Research, University of Antwerp, 2020 Antwerp, Belgium*

Eduard Fron − *Department of Chemistry, KU Leuven, 3001 Heverlee, Belgium;* orcid.org/0000-0003-2260-0798

Sara Bals − *Electron Microscopy for Materials Research, University of Antwerp, 2020 Antwerp, Belgium;* orcid.org/0000-0002-4249-8017

Johan Hofkens − *Department of Chemistry, KU Leuven, 3001 Heverlee, Belgium; Max Planck Institute for Polymer Research, 55128 Mainz, Germany;* orcid.org/0000-0002-9101-0567

Elke Debroye − *Department of Chemistry, KU Leuven, 3001 Heverlee, Belgium;* orcid.org/0000-0003-1087-4759

Complete contact information is available at: https://pubs.acs.org/10.1021/acsphotonics.1c01351

Author Contributions

#A.M. and B.P. contributed equally

Notes

The authors declare no competing financial interest.

ACKNOWLEDGMENTS

A.M. is thankful to IIT Mandi for his fellowship and Advanced Materials Research Centre for the experimental facilities. A.M. is also thankful to Torbjörn Pascher (Pascher Instrument) for writing the Z-scan data acquisition program. J.H. acknowledges financial support from the Research Foundation-Flanders (FWO, Grant No. G983.19N, G0A5817N, and G0H6316N) and the Flemish government through long-term structural funding Methusalem (CASAS2, Meth/15/04). B.P. acknowledges postdoctoral fellowship from the Research Foundation-Flanders (FWO Grant No. 1275521N). D.K. acknowledges the financial support from Science and Engineering Research Board (Grant No. PDF/2018/003146), India. N.J.S. acknowledges financial support from the Research Foundation-Flanders via a postdoctoral fellowship (FWO Grant No. 1238622N).

REFERENCES

(1) Liang, G.; Hu, X.; Yu, X.; Shen, Y.; Li, L. H.; Davies, A. G.; Linfield, E. H.; Liang, H. K.; Zhang, Y.; Yu, S. F.; Wang, Q. J. Integrated Terahertz Graphene Modulator with 100% Modulation Depth. *ACS Photonics* **2015**, *2* (11), 1559−1566.

(2) Mascheck, M.; Schmidt, S.; Silies, M.; Yatsui, T.; Kitamura, K.; Ohtsu, M.; Leipold, D.; Runge, E.; Lienau, C. Observing the localization of light in space and time by ultrafast second-harmonic microscopy. *Nat. Photonics* **2012**, *6* (5), 293−298.

(3) Song, Y.; Chen, Y.; Jiang, X.; Ge, Y.; Wang, Y.; You, K.; Wang, K.; Zheng, J.; Ji, J.; Zhang, Y.; Li, J.; Zhang, H. Nonlinear Few-Layer MXene-Assisted All-Optical Wavelength Conversion at Telecommunication Band. *Adv. Opt. Mater.* **2019**, *7* (18), 1801777.

(4) Nayak, A.; Park, J.; De Mey, K.; Hu, X.; Duncan, T. V.; Beratan, D. N.; Clays, K.; Therien, M. J. Large Hyperpolarizabilities at Telecommunication-Relevant Wavelengths in Donor-Acceptor-Donor Nonlinear Optical Chromophores. *ACS Cent. Sci.* **2016**, *2* (12), 954−966.

(5) Ye, W.; Zeuner, F.; Li, X.; Reineke, B.; He, S.; Qiu, C.-W.; Liu, J.; Wang, Y.; Zhang, S.; Zentgraf, T. Spin and wavelength multiplexed nonlinear metasurface holography. *Nat. Commun.* **2016**, *7* (1), 11930.
(6) Xu, J.; Li, X.; Xiong, J.; Yuan, C.; Semin, S.; Rasing, T.; Bu, X. H. Halide Perovskites for Nonlinear Optics. *Adv. Mater.* **2020**, *32* (3), 1806736.
(7) Shi, J.; Yu, P.; Liu, F.; He, P.; Wang, R.; Qin, L.; Zhou, J.; Li, X.; Zhou, J.; Sui, X.; Zhang, S.; Zhang, Y.; Zhang, Q.; Sum, T. C.; Qiu, X.; Liu, Z.; Liu, X. 3R MoS_2 with Broken Inversion Symmetry: A Promising Ultrathin Nonlinear Optical Device. *Adv. Mater.* **2017**, *29* (30), 1701486.
(8) Quan, C.; Lu, C.; He, C.; Xu, X.; Huang, Y.; Zhao, Q.; Xu, X. Band Alignment of $MoTe_2/MoS_2$ Nanocomposite Films for Enhanced Nonlinear Optical Performance. *Adv. Mater. Interfaces* **2019**, *6* (5), 1801733.
(9) Zhao, M.; Peng, R.; Zheng, Q.; Wang, Q.; Chang, M.-J.; Liu, Y.; Song, Y.-L.; Zhang, H.-L. Broadband optical limiting response of a graphene-PbS nanohybrid. *Nanoscale* **2015**, *7* (20), 9268−9274.
(10) Zheng, C.; Lei, L.; Huang, J.; Chen, W.; Li, W.; Wang, H.; Huang, L.; Huang, D. Facile control of metal nanoparticles from isolated nanoparticles to aggregated clusters on two-dimensional graphene to form optical limiters. *J. Mater. Chem. C* **2017**, *5* (44), 11579−11589.
(11) Zhao, G.; Zhang, F.; Wu, Y.; Hao, X.; Wang, Z.; Xu, X. One-Step Exfoliation and Hydroxylation of Boron Nitride Nanosheets with Enhanced Optical Limiting Performance. *Adv. Opt. Mater.* **2016**, *4* (1), 141−146.
(12) Shi, J.-m.; Xu, W.; Liu, Q.-y.; Liu, F.-l.; Huang, Z.-l.; Lei, H.; Yu, W.-t.; Fang, Q. Polynitrile-bridged two-dimensional crystal: Eu(iii) complex with strong fluorescence emission and NLO property. *Chem. Commun.* **2002**, No. 7, 756−757.
(13) Wang, C.; Zhang, T.; Lin, W. Rational Synthesis of Noncentrosymmetric Metal-Organic Frameworks for Second-Order Nonlinear Optics. *Chem. Rev.* **2012**, *112* (2), 1084−1104.
(14) Ravindran, S.; Datta, A.; Alameh, K.; Lee, Y. T. GaAs based long-wavelength microring resonator optical switches utilising bias assisted carrier-injection induced refractive index change. *Opt. Express* **2012**, *20* (14), 15610−15627.
(15) Geldenhuys, R.; van der Merwe, J. S.; Thakulsukanant, K.; Wang, Z.; Chi, N.; Yu, S. Contention resolution and variable length optical packet switching using the active vertical-coupler-based optical Crosspoint switch. *Opt. Switch. Netw* **2011**, *8* (2), 86−92.
(16) Shin, S.; Su, C. Strong increase of the derivative of the carrier-induced index change of semiconductor lasers at low injected carrier density. *IEEE Photonics Technol. Lett.* **1993**, *5* (9), 981−983.
(17) Miller, A.; Welford, K.; Daino, B. *Nonlinear Optical Materials and Devices for Applications in Information Technology*; Springer Science & Business Media, 2013; Vol. *289*.
(18) Zhou, Y.; Huang, Y.; Xu, X.; Fan, Z.; Khurgin, J. B.; Xiong, Q. Nonlinear optical properties of halide perovskites and their applications. *Appl. Phys. Rev.* **2020**, *7* (4), 041313.
(19) Walters, G.; Sargent, E. H. Electro-optic Response in Germanium Halide Perovskites. *J. Phys. Chem. Lett.* **2018**, *9* (5), 1018−1027.
(20) Manser, J. S.; Christians, J. A.; Kamat, P. V. Intriguing Optoelectronic Properties of Metal Halide Perovskites. *Chem. Rev.* **2016**, *116* (21), 12956−13008.
(21) Stranks, S. D.; Hoye, R. L. Z.; Di, D.; Friend, R. H.; Deschler, F. The Physics of Light Emission in Halide Perovskite Devices. *Adv. Mater.* **2019**, *31* (47), 1803336.
(22) Galkowski, K.; Mitioglu, A.; Miyata, A.; Plochocka, P.; Portugall, O.; Eperon, G. E.; Wang, J. T.-W.; Stergiopoulos, T.; Stranks, S. D.; Snaith, H. J.; Nicholas, R. J. Determination of the exciton binding energy and effective masses for methylammonium and formamidinium lead tri-halide perovskite semiconductors. *Energy Environ. Sci.* **2016**, *9* (3), 962−970.
(23) Qi, X.; Zhang, Y.; Ou, Q.; Ha, S. T.; Qiu, C.-W.; Zhang, H.; Cheng, Y.-B.; Xiong, Q.; Bao, Q. Photonics and Optoelectronics of 2D Metal-Halide Perovskites. *Small* **2018**, *14* (31), 1800682.
(24) Jiang, G.; Miao, L.; Yi, J.; Huang, B.; Peng, W.; Zou, Y.; Huang, H.; Hu, W.; Zhao, C.; Wen, S. Ultrafast pulse generation from erbium-doped fiber laser modulated by hybrid organic-inorganic halide perovskites. *Appl. Phys. Lett.* **2017**, *110* (16), 161111.
(25) Li, P.; Chen, Y.; Yang, T.; Wang, Z.; Lin, H.; Xu, Y.; Li, L.; Mu, H.; Shivananju, B. N.; Zhang, Y.; Zhang, Q.; Pan, A.; Li, S.; Tang, D.; Jia, B.; Zhang, H.; Bao, Q. Two-Dimensional $CH_3NH_3PbI_3$ Perovskite Nanosheets for Ultrafast Pulsed Fiber Lasers. *ACS Appl. Mater. Interfaces* **2017**, *9* (14), 12759−12765.
(26) Dohner, E. R.; Jaffe, A.; Bradshaw, L. R.; Karunadasa, H. I. Intrinsic White-Light Emission from Layered Hybrid Perovskites. *J. Am. Chem. Soc.* **2014**, *136* (38), 13154−13157.
(27) Li, X.; Wu, Y.; Zhang, S.; Cai, B.; Gu, Y.; Song, J.; Zeng, H. $CsPbX_3$ Quantum Dots for Lighting and Displays: Room-Temperature Synthesis, Photoluminescence Superiorities, Underlying Origins and White Light-Emitting Diodes. *Adv. Funct. Mater.* **2016**, *26* (15), 2435−2445.
(28) Wang, Y.; Li, X.; Zhao, X.; Xiao, L.; Zeng, H.; Sun, H. Nonlinear Absorption and Low-Threshold Multiphoton Pumped Stimulated Emission from All-Inorganic Perovskite Nanocrystals. *Nano Lett.* **2016**, *16* (1), 448−453.
(29) He, T.; Li, J.; Ren, C.; Xiao, S.; Li, Y.; Chen, R.; Lin, X. Strong two-photon absorption of Mn-doped CsPbCl3 perovskite nanocrystals. *Appl. Phys. Lett.* **2017**, *111* (21), 211105.
(30) Han, X.; Zheng, Y.; Chai, S.; Chen, S.; Xu, J. 2D organic-inorganic hybrid perovskite materials for nonlinear optics. *Nanophotonics* **2020**, *9* (7), 1787−1810.
(31) Yi, J.; Miao, L.; Li, J.; Hu, W.; Zhao, C.; Wen, S. Third-order nonlinear optical response of CH_3 NH_3 PbI_3 perovskite in the mid-infrared regime. *Opt. Mater. Express* **2017**, *7* (11), 3894−3901.
(32) Ketavath, R.; Katturi, N. K.; Ghugal, S. G.; Kolli, H. K.; Swetha, T.; Soma, V. R.; Murali, B. Deciphering the Ultrafast Nonlinear Optical Properties and Dynamics of Pristine and Ni-Doped $CsPbBr_3$ Colloidal Two-Dimensional Nanocrystals. *J. Phys. Chem. Lett.* **2019**, *10* (18), 5577−5584.
(33) Noel, N. K.; Stranks, S. D.; Abate, A.; Wehrenfennig, C.; Guarnera, S.; Haghighirad, A.-A.; Sadhanala, A.; Eperon, G. E.; Pathak, S. K.; Johnston, M. B.; Petrozza, A.; Herz, L. M.; Snaith, H. J. Lead-free organic-inorganic tin halide perovskites for photovoltaic applications. *Energy Environ. Sci.* **2014**, *7* (9), 3061−3068.
(34) Hao, F.; Stoumpos, C. C.; Cao, D. H.; Chang, R. P. H.; Kanatzidis, M. G. Lead-free solid-state organic-inorganic halide perovskite solar cells. *Nat. Photonics* **2014**, *8* (6), 489−494.
(35) Jellicoe, T. C.; Richter, J. M.; Glass, H. F. J.; Tabachnyk, M.; Brady, R.; Dutton, S. E.; Rao, A.; Friend, R. H.; Credgington, D.; Greenham, N. C.; Böhm, M. L. Synthesis and Optical Properties of Lead-Free Cesium Tin Halide Perovskite Nanocrystals. *J. Am. Chem. Soc.* **2016**, *138* (9), 2941−2944.
(36) Leng, M.; Chen, Z.; Yang, Y.; Li, Z.; Zeng, K.; Li, K.; Niu, G.; He, Y.; Zhou, Q.; Tang, J. Lead-Free, Blue Emitting Bismuth Halide Perovskite Quantum Dots. *Angew. Chem., Int. Ed.* **2016**, *55* (48), 15012−15016.
(37) Zhang, J.; Yang, Y.; Deng, H.; Farooq, U.; Yang, X.; Khan, J.; Tang, J.; Song, H. High Quantum Yield Blue Emission from Lead-Free Inorganic Antimony Halide Perovskite Colloidal Quantum Dots. *ACS Nano* **2017**, *11* (9), 9294−9302.
(38) Mushtaq, A.; Kushavah, D.; Ghosh, S.; Pal, S. K. Nonlinear optical properties of benzylamine lead(II) bromide perovskite microdisks in femtosecond regime. *Appl. Phys. Lett.* **2019**, *114* (5), 051902.
(39) Gray, M. B.; Majher, J. D.; Strom, T. A.; Woodward, P. M. Broadband White Emission in $Cs_2AgIn_{1-x}Bi_xCl_6$ Phosphors. *Inorg. Chem.* **2019**, *58* (19), 13403−13410.
(40) Yang, B.; Mao, X.; Hong, F.; Meng, W.; Tang, Y.; Xia, X.; Yang, S.; Deng, W.; Han, K. Lead-Free Direct Band Gap Double-Perovskite Nanocrystals with Bright Dual-Color Emission. *J. Am. Chem. Soc.* **2018**, *140* (49), 17001−17006.
(41) Luo, J.; Li, S.; Wu, H.; Zhou, Y.; Li, Y.; Liu, J.; Li, J.; Li, K.; Yi, F.; Niu, G.; Tang, J. $Cs_2AgInCl_6$ Double Perovskite Single Crystals:

https://doi.org/10.1021/acsphotonics.1c01351
ACS Photonics XXXX, XXX, XXX−XXX

Parity Forbidden Transitions and Their Application For Sensitive and Fast UV Photodetectors. *ACS Photonics* **2018**, *5* (2), 398−405.
(42) Krishnakanth, K. N.; Seth, S.; Samanta, A.; Venugopal Rao, S. Broadband ultrafast nonlinear optical studies revealing exciting multi-photon absorption coefficients in phase pure zero-dimensional Cs_4PbBr_6 perovskite films. *Nanoscale* **2019**, *11* (3), 945−954.
(43) Philip, R.; Chantharasupawong, P.; Qian, H.; Jin, R.; Thomas, J. Evolution of Nonlinear Optical Properties: From Gold Atomic Clusters to Plasmonic Nanocrystals. *Nano Lett.* **2012**, *12* (9), 4661−4667.
(44) Tripathy, U.; Bisht, P. B. Simultaneous estimation of optical nonlinear refractive and absorptive parameters by solvent induced changes in optical density. *Opt. Commun.* **2006**, *261* (2), 353−358.
(45) Mukundam, V.; Sa, S.; Kumari, A.; Das, R.; Venkatasubbaiah, K. B-N coordinated triaryl pyrazole: effect of dimerization, and optical and NLO properties. *J. Mater. Chem. C* **2019**, *7* (40), 12725−12737.
(46) Kinastowska, K.; Piela, K.; Gordel, M.; Żak, A.; Kołkowski, R.; Samoć, M. Gold nanoparticle-decorated graphene as a nonlinear optical material in the visible and near-infrared spectral range. *Phys. Chem. Chem. Phys.* **2018**, *20* (27), 18862−18872.
(47) Ekbote, A.; Patil, P. S.; Maidur, S. R.; Chia, T. S.; Quah, C. K. Structural, third-order optical nonlinearities and figures of merit of (E)-1-(3-substituted phenyl)-3-(4-fluorophenyl) prop-2-en-1-one under CW regime: New chalcone derivatives for optical limiting applications. *Dyes Pigm.* **2017**, *139*, 720−729.
(48) Liu, F.; Marongiu, D.; Pau, R.; Sarritzu, V.; Wang, Q.; Lai, S.; Lehmann, A. G.; Quochi, F.; Saba, M.; Mura, A.; Bongiovanni, G.; Mattoni, A.; Caddeo, C.; Bosin, A.; Filippetti, A. Ag/In lead-free double perovskites. *EcoMat* **2020**, *2* (1), No. e12017.
(49) Pan, L.; Tamai, N.; Kamada, K.; Deki, S. Nonlinear optical properties of thiol-capped CdTe quantum dots in nonresonant region. *Appl. Phys. Lett.* **2007**, *91* (5), 051902.
(50) Li, J.; Ren, C.; Qiu, X.; Lin, X.; Chen, R.; Yin, C.; He, T. Ultrafast optical nonlinearity of blue-emitting perovskite nanocrystals. *Photonics Res.* **2018**, *6* (6), 554−559.
(51) Wang, Y.; Yang, X.; He, T. C.; Gao, Y.; Demir, H. V.; Sun, X. W.; Sun, H. D. Near resonant and nonresonant third-order optical nonlinearities of colloidal InP/ZnS quantum dots. *Appl. Phys. Lett.* **2013**, *102* (2), 021917.
(52) Zheng, X.; Zhang, Y.; Chen, R.; Cheng, X.; Xu, Z.; Jiang, T. Z-scan measurement of the nonlinear refractive index of monolayer WS_2. *Opt. Express* **2015**, *23* (12), 15616−15623.
(53) Bulutay, C.; Turgut, C. M.; Zakhleniuk, N. A. Carrier-induced refractive index change and optical absorption in wurtzite InN and GaN: Full-band approach. *Phys. Rev. B: Condens. Matter Mater. Phys.* **2010**, *81* (15), 155206.
(54) Krishnakanth, K. N.; Seth, S.; Samanta, A.; Rao, S. V. Broadband femtosecond nonlinear optical properties of $CsPbBr_3$ perovskite nanocrystals. *Opt. Lett.* **2018**, *43* (3), 603−606.
(55) Han, Q.; Wu, W.; Liu, W.; Yang, Q.; Yang, Y. Two-photon absorption and upconversion luminescence of colloidal $CsPbX_3$ quantum dots. *Opt. Mater.* **2018**, *75*, 880−886.
(56) Zou, S.; Yang, G.; Yang, T.; Zhao, D.; Gan, Z.; Chen, W.; Zhong, H.; Wen, X.; Jia, B.; Zou, B. Template-Free Synthesis of High-Yield Fe-Doped Cesium Lead Halide Perovskite Ultralong Microwires with Enhanced Two-Photon Absorption. *J. Phys. Chem. Lett.* **2018**, *9* (17), 4878−4885.
(57) Chen, W.; Zhang, S.; Zhou, M.; Zhao, T.; Qin, X.; Liu, X.; Liu, M.; Duan, P. Two-Photon Absorption-Based Upconverted Circularly Polarized Luminescence Generated in Chiral Perovskite Nanocrystals. *J. Phys. Chem. Lett.* **2019**, *10* (12), 3290−3295.
(58) Walters, G.; Sutherland, B. R.; Hoogland, S.; Shi, D.; Comin, R.; Sellan, D. P.; Bakr, O. M.; Sargent, E. H. Two-Photon Absorption in Organometallic Bromide Perovskites. *ACS Nano* **2015**, *9* (9), 9340−9346.
(59) Wu, W.; Chai, Z.; Gao, Y.; Kong, D.; He, F.; Meng, X.; Wang, Y. Carrier dynamics and optical nonlinearity of alloyed CdSeTe quantum dots in glass matrix. *Opt. Mater. Express* **2017**, *7* (5), 1547−1556.
(60) Lad, A. D.; Kiran, P. P.; More, D.; Kumar, G. R.; Mahamuni, S. Two-photon absorption in ZnSe and ZnSe/ZnS core/shell quantum structures. *Appl. Phys. Lett.* **2008**, *92* (4), 043126.
(61) Mary, K. A. A.; Unnikrishnan, N. V.; Philip, R. Role of surface states and defects in the ultrafast nonlinear optical properties of CuS quantum dots. *APL Mater.* **2014**, *2* (7), 076104.
(62) Said, A. A.; Sheik-Bahae, M.; Hagan, D. J.; Wei, T. H.; Wang, J.; Young, J.; Van Stryland, E. W. Determination of bound-electronic and free-carrier nonlinearities in ZnSe, GaAs, CdTe, and ZnTe. *J. Opt. Soc. Am. B* **1992**, *9* (3), 405−414.
(63) Van Stryland, E. W.; Vanherzeele, H.; Woodall, M. A.; Soileau, M.; Smirl, A. L.; Guha, S.; Boggess, T. F. Two photon absorption, nonlinear refraction, and optical limiting in semiconductors. *Opt. Eng.* **1985**, *24* (4), 244613.
(64) Gu, B.; Fan, Y.-X.; Chen, J.; Wang, H.-T.; He, J.; Ji, W. Z-scan theory of two-photon absorption saturation and experimental evidence. *J. Appl. Phys.* **2007**, *102* (8), 083101.

https://doi.org/10.1021/acsphotonics.1c01351
ACS Photonics XXXX, XXX, XXX−XXX